ELSEVIER

Check for updates

Antiviral activity against Middle East Respiratory Syndrome coronavirus by Montelukast, an anti-asthma drug

Hanjie Jonathan Gan [a], Amaravadhi Harikishore [a], Jihye Lee [b], Sangeun Jeon [b], Sreekanth Rajan [a], Ming Wei Chen [a], Jun Long Neo [a], Seungtaek Kim [b,**], Ho Sup Yoon [a,*]

[a] School of Biological Sciences, Nanyang Technological University, 60 Nanyang Drive, 637551, Singapore
[b] Zoonotic Virus Laboratory, Institut Pasteur Korea, Seongnam, South Korea

ARTICLE INFO

ABSTRACT

Middle East Respiratory Syndrome (MERS) is a respiratory disease caused by a coronavirus (MERS-CoV). Since its emergence in 2012, nosocomial amplifications have led to its high epidemic potential and mortality rate of 34.5%. To date, there is an unmet need for vaccines and specific therapeutics for this disease. Available treatments are either supportive medications in use for other diseases or those lacking specificity requiring higher doses. The viral infection mode is initiated by the attachment of the viral spike glycoprotein to the human Dipeptidyl Peptidase IV (DPP4). Our attempts to screen antivirals against MERS led us to identify montelukast sodium hydrate (MSH), an FDA-approved anti-asthma drug, as an agent attenuating MERS-CoV infection. We showed that MSH directly binds to MERS-CoV-Receptor-Binding Domain (RBD) and inhibits its molecular interaction with DPP4 in a dose-dependent manner. Our cell-based inhibition assays using MERS pseudovirions demonstrated that viral infection was significantly inhibited by MSH and was further validated using infectious MERS-CoV culture. Thus, we propose MSH as a potential candidate for therapeutic developments against MERS-CoV infections.

1. Introduction

Middle East Respiratory Syndrome (MERS) emerged in 2012, extending its spread from Saudi Arabia, Qatar, and Jordan to 27 different countries (Sharif-Yakan and Kanj, 2014; WHO, 2020; Zaki et al., 2012). Subsequently, it was found to be a coronavirus (CoV) infection that has undergone nosocomial amplifications contributing to its spread (Majumder et al., 2017). To date, there are a total of 2494 lab-confirmed cases and 858 deaths resulting from MERS, leading to a high mortality rate of 34.5%. There are currently no available vaccines or therapeutics specific to MERS. Treatment is mostly supportive, and broad-spectrum therapeutics were previously used for severe cases (CDC, 2015; WHO, 2018). However, the lack of specificity and the need for high dosages to exert any therapeutic effect resulted in adverse side effects such as ribavirin-induced anemia and carcinogenicity (Dyall et al., 2014). Therefore, due to this unmet need for more effective treatments and its high epidemic potential, MERS-CoV is placed on the list of priority diseases and pathogens for critical research and development by the World Health Organization (WHO) (WHO, 2018).

Until today, vaccine development against MERS led to the identification of potential candidates such as DNA vaccines and antibodies that are in clinical trials and preclinical phases (Cho et al., 2018; Perlman and Vijay, 2016; Zhang et al., 2014; Zhou et al., 2019). Although vaccine development is critical in combating infectious diseases, concurrent research on therapeutic development is still required to address the need for targeted treatment options. As such, our study prioritizes the development of inhibitors against the viral-host interface to suppress viral progression. For this, the primary focus was on the 204-residue long viral receptor-binding domain (RBD) on the S1 glycoprotein of MERS-CoV, which interacts with its host cell receptor: Dipeptidyl peptidase IV (DPP4) (Wang et al., 2013).

Within the S1 glycoprotein, RBD was found to interact with DPP4 by mutation studies (Du et al., 2013; Wang et al., 2013; Zhang et al., 2014). More importantly, the crystal structure of MERS-CoV RBD-DPP4

complex revealed the precise molecular basis of the MERS-CoV RBD-DPP4 interface. A unique feature of the interaction is the binding of MERS-CoV RBD to DPP4 at blades 4 and 5 of the β-propeller domain exposed to the surface, instead of its canonical catalytic site (Wang et al., 2013). Consistent with other studies, it provided a probable explanation for DPP4 inhibitors' ineffectiveness in blocking this viral attachment (Raj et al., 2013). Anyhow, the MERS-CoV RBD-DPP4 complex structure directed the targeting of this interface region as the probable inhibition site of viral attachment and thereby its entry.

In this direction, we studied the MERS-CoV RBD-DPP4 complex interface and screened potential therapeutic drugs for MERS. The crystal structure of MERS-CoV RBD-DPP4 complex suggests that MERS-CoV RBD recognizes its cognate receptor DPP4 at a different site from the catalytic/sitagliptin binding site in DPP4. MERS-CoV RBD was found to interact with residues ranging from 281 to 296 of DPP4. Along this 15-amino acid stretch, a short helical region (residues 290–296) of DPP4 fits nicely into RBD's hydrophobic surface pocket. Thus, in this study, we targeted the protein-protein interactions harboring the RBD's hydrophobic pocket (Y540-Q544, W553–S557, N501-D510 residues) that anchored the short helix region at the binding site to disrupt receptor recognition of and thereby prevent viral entry into host cells. Based on the PLP fitness scores and the molecular interactions at the MERS-CoV RBD residues as mentioned above, seven FDA-approved drugs were selected to evaluate *in vitro* binding and cell-based viral entry assays. Through *in vitro* fluorescence quenching and thermofluor titrations, Montelukast Sodium Hydrate (MSH) (NCBI, 2020; Song et al., 2018) was found to interact with MERS-CoV RBD in a dose-dependent manner. Subsequently, assays using MERS pseudovirions revealed significant inhibition of viral entry by MSH. Further validation was then performed using an infectious virus culture (MERS-CoV/EMC/2012) (CDC, 2015; Park et al., 2017).

2. Materials and methods

2.1. In silico screening targeting MERS-CoV RBD-DPP4 interface

The crystal structure of MERS-CoV RBD-DPP4 (PDB: 4L72) was employed to virtually screen the FDA approved library dataset. The protein subunits of the complex structure were prepared by removing the heteroatoms, adjusting the charges, potentials, bond orders, and missing atoms with CHARMM force field and energy minimized with heavy atom constraint for 5000 steps of conjugate gradient algorithm in Biovia Discovery Studio 4.0 (Dassault Systèmes, 2016). Thus, the minimized protein is used for further molecular docking simulation studies. 3D coordinates of ligands in the FDA approved library were obtained from the Zinc database (Sterling and Irwin, 2015). The ligands were energy minimized using the smart minimizer algorithm, and this minimized library was taken into molecular docking studies. Molecular studies were carried out using GOLD, CCDC suite of programs (Jones et al., 1997). As there were no known ligands characterized for this protein, default docking parameters were employed to generate docking poses for the ligands from the FDA-approved library. All modeling and simulation studies were carried on a Linux Workstation.

2.2. Expression and purification of recombinant proteins

pFastBac DUAL vectors containing the MERS-CoV RBD and DPP4 constructs were kindly gifted by Professor Xinquan Wang. Truncations were performed on the RBD construct to shorten the target sequences to the reported critical region for downstream analyses (Wang et al., 2013) before cloning into a pFastBac-Sec-NH vector. Thereafter, transposition, isolation of bacmids, and subsequent bacmid transfection for the generation of RBD and DPP4 baculoviruses were systematically conducted. The low-titer P_1 baculovirus stocks were amplified to high-titer P_3 baculovirus stocks before the expression of recombinant proteins.

For recombinant protein expression, baculoviruses were used to infect *sf9* cells at a seeding density of 2.5×10^6 cells/mL. Cells were then incubated for 72 h in a shaking incubator at 27 °C at 130 rpm, protected from light before harvesting. The culture was then subjected to centrifugation at $9,000 \times g$ for 15 min, and the supernatant containing the soluble secreted proteins were purified by Ni^{2+}-NTA affinity chromatography. The elution fractions were collected, concentrated, and injected for secondary purifications via the HiLoad Superdex 75 16/60 and Superdex 200 Increase 10/300 GL columns.

Maltose-binding protein (MBP) tagged MERS-CoV RBD wild type (WT), and mutant constructs (V555A, R542D, and Y540A) were cloned into pHLmMBP-10 vector and subsequently transfected using Expifectamine 293 (Gibco) transfection reagent and expressed in ExPi293 cells. The culture was incubated at 37 °C at 120 rpm for 120 h before harvesting. The culture was then subjected to centrifugation at $3,000 \times g$, and the supernatant containing the soluble secreted proteins were purified by Ni^{2+}-NTA affinity chromatography. The elution fractions were collected, concentrated, and injected for secondary purifications via the HiLoad Superdex 200 16/60 column.

2.3. Protein Identity (Protein ID) confirmation and functionality test

Purified recombinant proteins were analyzed by SDS-PAGE on a 10% SDS-gel. Bands of interest were extracted and sent for MALDI-TOF Mass Spectroscopy Protein ID analysis. Binding of the recombinant MERS-CoV RBD with its host cell receptor, DPP4, was performed to assess its functionality. The purified RBD and DPP4 proteins were incubated at 4 °C for 2 h before injecting into a Superdex 200 Increase 10/300 GL column for analysis. Negative control runs were prepared beforehand with DPP4 only, and MERS-CoV RBD only samples for comparison (Suppl. Figure 2).

2.4. Intrinsic Fluorescence Quenching

Purified MERS-CoV RBD samples were centrifuged at $16,000 \times g$ for 10 min to pellet down any aggregates. The protein sample was diluted in 25 mM Tris-HCl (pH 8.0), 30 mM NaCl and 0.01% NaN_3 to a final concentration of 5 μM per well in a Corning® 96 well, flat bottom black plate. Ligands diluted in Dimethyl Sulfoxide (DMSO) were added into each well at a protein to ligand ratio of 1:5. DMSO was added in place of the ligands for the negative control. Subsequent screens were carried out for a protein to ligand ratio of 1:5, 1:10, 1:20, 1:30, and 1:40.

The plate was then loaded onto a Tecan Safire^2 ™ microplate reader for endpoint measurements. The absorption wavelength was pre-set at 290 nm, and the emission range was set between 290 and 430 nm, respectively. Quenching data was first baseline corrected and fitted into a non-linear regression Gaussian model using the following equation: Y=Amplitude*exp (-0.5*((X-Mean)/SD)^2). Then, the amplitude of each sample was recorded and transformed to fit a saturation curve. The K_D was then calculated using the following equation: Y=Bmax*X/(K_D + X) using Prism8.

2.5. Differential Scanning Fluorimetry (DSF)

Purified MBP-tagged MERS-CoV RBD was diluted in 25 mM Tris-HCl (pH 8.0), 30 mM NaCl and 0.01% NaN_3 to a final concentration of 0.2 mg/ml per well in a Framestar® 96, semi-skirted PCR plate (4titude, Surrey). 9 two-fold serial dilutions were conducted for MSH in DMSO, from a final concentration of 100 μM down to 195 nM. DMSO was added in place of MSH for the control set. SYPRO Orange dye (Life Technologies, CA) was then added into each well to a final concentration of 1x. The plate was then sealed with a MicroAmp® Optical Adhesive Film from Applied Biosystems (Life Technologies, CA) and loaded into the Applied Biosystems® 7500 Real-Time PCR System. The system was initiated with a temperature increase from 25 °C to 95 °C, with a ramp in 0.5 °C per 5 s and plate-reads with respective temperature increments. The absorption and emission wavelengths were measured at 490 and
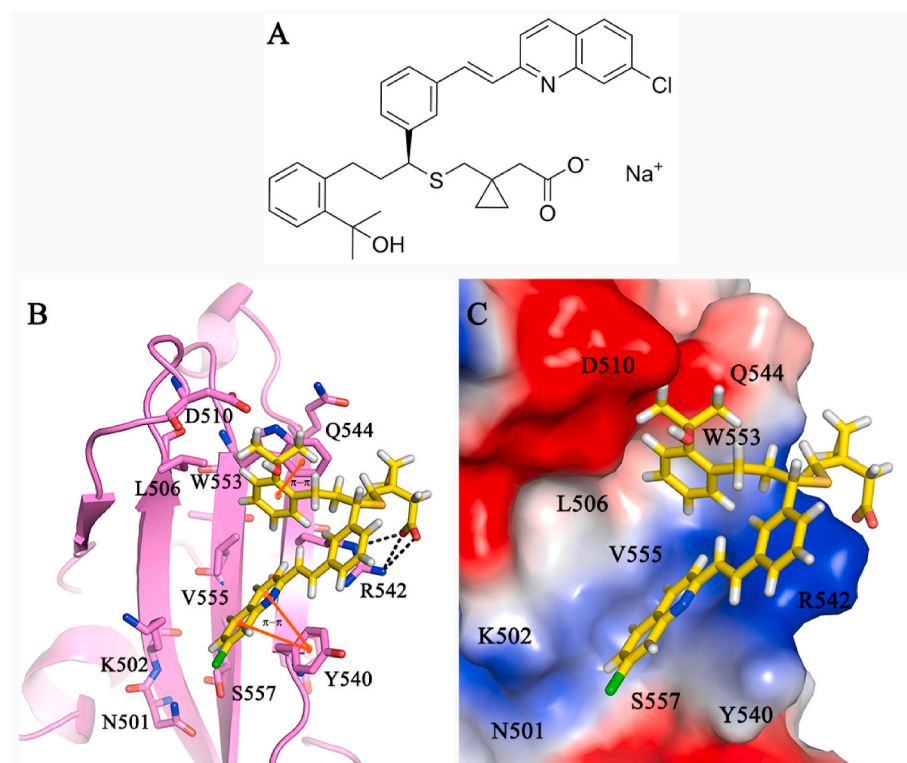
Fig. 1. *In silico* screening on the molecular interaction model of MSH with MERS-CoV RBD. (A) Chemical structure of MSH. (B) Cartoon model highlighting molecular interactions of MSH. The salt bridge interactions (black dotted lines) between the acetic acid group of MSH and R542 residue of MERS-CoV RBD. The ligand-binding was further stabilized by (i) π-π stacking interactions (highlighted in orange lines) between the phenyl, chloroquinoline groups of MSH with W553, Y540 residues respectively, (ii) alkyl hydrophobic interactions with surrounding V555, CH_2 sidechain atoms of R542, K502, and S557 residues of MERS-CoV RBD. (C) Potential surface view of MSH binding position on MERS-CoV RBD.

575 nm, respectively. Data was processed and fitted to a Boltzmann sigmoidal model for melting temperature (T_m) analyses. Analysis of the thermofluor data was conducted on Prism8 using the equation: Y=Bottom + (Top-Bottom)/(1+(IC_{50}/X)^HillSlope).

2.6. Analytical gel filtration experiments

Samples were pre-incubated in 4 °C before the analytical gel filtration using a Superdex 200 Increase 10/300 GL column. For the two-sample conditions, (1) RBD was incubated with MSH overnight followed by incubation with DPP4 for 3 h, and (2) RBD-DPP4 was incubated for 3 h, followed by incubation with MSH overnight. The molar concentration of MSH 10-fold excess compared to the protein samples. The samples were monitored via Ultra-violet (UV) absorption at 280 nm, and shifts in fractionation peaks were analyzed.

2.7. Generation of MERS-Spike pseudovirions

MERS-Spike pseudovirions were designed and produced using a 3rd generation lentiviral pseudotyping system involving Envelope, Transfer, and Packaging vectors in HEK 293T cells (ATCC, VA). Prior to usage, viral supernatants were concentrated, and immunoblot analysis using an anti-MERS-S1 center antibody (Sino-Biological, CN) was conducted to detect the presence of MERS spike proteins. Infection assays were used to test the functionality as well as the target specificity of these pseudovirions on *Vero E6* cells (ATCC C1008, VA). Quantitative measurements were obtained via luciferase assay. Measurements were obtained using the Tecan Safire[2] ™ microplate reader. Luminescence data positively correlates to viral entry, and comparisons between untreated and treated wells were used for viral entry inhibition analysis.

2.8. Cell viability assay

Vero E6 cells were grown and maintained on a 10 cm^3 culture plate in Dulbecco's Modified Eagle Medium (DMEM) medium with high glucose and 4 mM L-glutamine, supplemented with 10% (v/v) fetal bovine serum (FBS) and 1% (v/v) 100x Penicillin-Streptomycin solution at 37 °C in a 5% humidified CO_2 incubator. To determine the highest non-toxic dose of MSH for subsequent assays, a cell viability assay using WST-1 reagent (Roche, CH) was performed on *Vero E6* cells with increasing MSH concentration. *Vero E6* cells were incubated at 37 °C for 48 h with MSH treatment to simulate inhibition assay conditions before adding WST-1 and measurements according to the Cell Proliferation Reagent WST-1 manufacturer's protocol.

2.9. Viral entry inhibition assay using MERS-Spike pseudovirions

MERS-Spike pseudovirions were pre-incubated with MSH for 30 min in room temperature before inoculation to *Vero E6* cells. Inoculums were left incubated with the cells at 37 °C up to 48 h before harvesting for luciferase measurements. Luminescence measurements were subjected to baseline-correction with the uninfected wells, and comparisons between untreated and treated wells were analyzed.

2.10. Assessment of the antiviral effect of MSH against infectious MERS-CoV

Vero cells (ATCC CCL-81, VA) were maintained in Dulbecco's Modified Eagle Medium (DMEM; Welgene) supplemented with 10% (v/v) fetal bovine serum (FBS) and 1% antibiotic-antimycotic solution (Life Technologies, CA) at 37 °C in a 5% humidified CO_2 incubator. For infection experiments, the cells were seeded at 1.2×10^4 cells per well in Opti-PRO™ SFM supplemented with 4 mM L-Glutamine and 1 × Antibiotic-Antimycotic (Life Technologies, CA) in black, clear-bottom, 384-well plates (Greiner Bio-One, Austria), and MERS-CoV was added at a multiplicity of infection (MOI) of 0.06. Chloroquine diphosphate (CQ; C6628) and lopinavir (LPV; S1380) were purchased (SelleckChem, TX) and used for controls. All the experiments with infectious MERS-CoV (MERS-CoV/EMC/2012) were performed with the enhanced Biosafety Level 3 (BSL-3) containment procedures at Institut Pasteur Korea approved for use by Korea Centers for Disease Control and Prevention (KCDC).
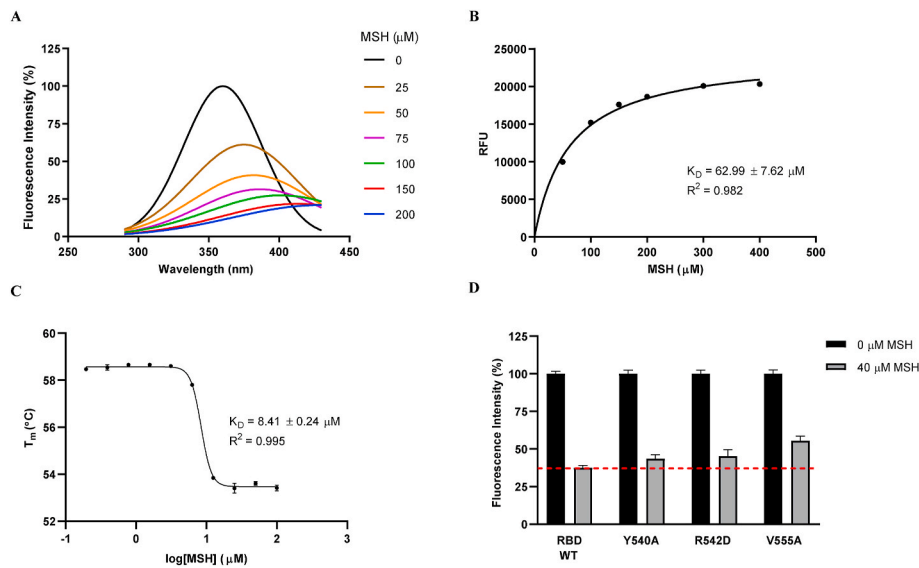
Fig. 2. MSH binds to MERS-CoV RBD in a dose-dependent manner. (A) Trp fluorescence quenching results of RBD and MSH, showing the extent of dose-dependent quenching from the comparison of peak heights and red-shift. Recombinant MERS-CoV RBD was used as control. (B) Binding curve plotted from quenching data of two independent assays. (C) RBD-MSH interaction analysis by Differential Scanning Fluorimetry (DSF). (D) Fluorescence quenching data on RBD mutants (V555A, R542D, Y540A) comparing the extent of quenching effect with MSH addition.

2.11. Immunofluorescent staining

The viral inoculums and drug treatments were incubated with the cells for 24 h. After this, the infected cells were fixed at 24 h post-infection (hpi) with 4% PFA and permeabilized with 0.25% Triton X-100 (Sigma Aldrich, USA) in Phosphate Buffer Saline (PBS) for 30 min. Infected cells were visualized by immunofluorescence of viral spike protein, which was detected by rabbit anti-MERS-CoV spike antibodies (Sino-Biological, CN), and cell viability was evaluated with Hoechst 33,342 (Thermo Fisher Scientific) stain. The immunofluorescence images were acquired using PerkinElmer Operetta (20x, Waltham, MA) and analyzed by the in-house Image Mining 3.0 (IM 3.0) software to quantify cell numbers and infection ratios. Antiviral activity was normalized to positive (mock) and negative (0.5% DMSO) controls in each assay plate. Dose-response curves (DRCs) were fitted by sigmoidal dose-response models, with the following equation: $Y = \text{Bottom} + (\text{Top} - \text{Bottom})/(1 + (IC_{50}/X)^{\text{Hillslope}})$, using XLfit 4 Software or Prism7. IC_{50} values were calculated from the normalized activity dataset-fitted curves. The IC_{50} and CC_{50} values were determined in duplicate experiments, and the selective index (SI) was calculated ($SI = CC_{50}/IC_{50}$).

2.12. Statistical analysis

For assays with three or more data sets compared to the control as a reference, One-way ANOVA statistical analyses were performed with Dunnett's Post-hoc test to compare all columns with the control column. In experiments with fewer than 3 data sets, an unpaired one-tailed *t*-test was conducted instead. $*p < 0.05$, $**p < 0.01$, $***p < 0.001$.

3. Results

3.1. In silico structure-guided screening targeting MERS-CoV RBD-DPP4 interface

Based on our *in silico* screening, one of the best fitting ligand, Montelukast Sodium Hydrate (MSH) (NCBI, 2020), was predicted to interact with MERS-CoV RBD with a good PLP fitness score of 85.2. Chemically, MSH is referred to as (R,E)-2-(1-(((1-(3-(2-(7-chloroquinolin-2-yl)vinyl)phenyl)-3-(2-(2-hydroxypropan-2-yl)phenyl)propyl)thio)methyl)cyclopropyl)acetic acid (Fig. 1A). The carboxyl moiety on the thio-methyl-cyclopropyl-acetic acid fragment of MSH was found to be involved in salt bridge interactions (black dotted lines) with side chain –NH atoms of R542, while the phenyl group of 3-(2-(2-hydroxypropan-2-yl) phenyl) propyl fragment was involved in π-π stacking interactions with W553 residue. The ligand-binding was further stabilized by strong π-π stacking interaction of 7-chloroquinoline moiety with Y540 and hydrophobic interactions with V555, sidechain CH_2 atoms of K502, R542, and S557 residues. (Fig. 1B and C).
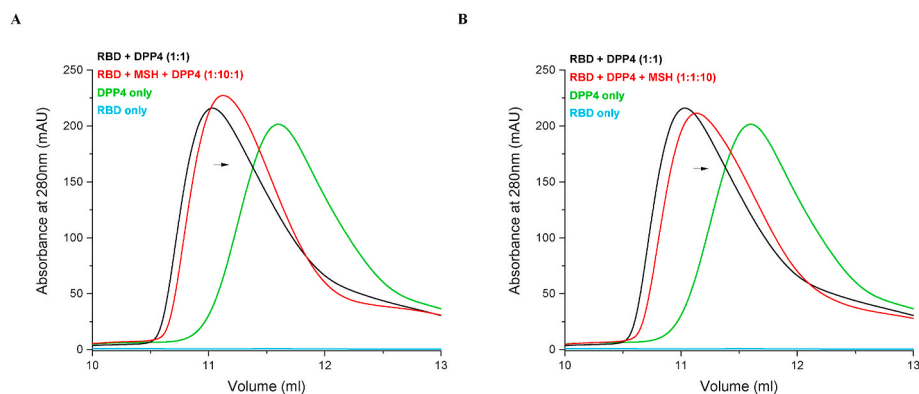
Fig. 3. Potential effects on MERS-CoV RBD-DPP4 complex formation inhibition and complex dissociation by MSH. Analytical gel filtration chromatography experiments exhibited slight but distinct and consistent peak shifts from RBD-DPP4 complex peak towards DPP4 only peak in (A) RBD + MSH followed by the addition of DPP4 and (B) RBD-DPP4 complex + MSH.
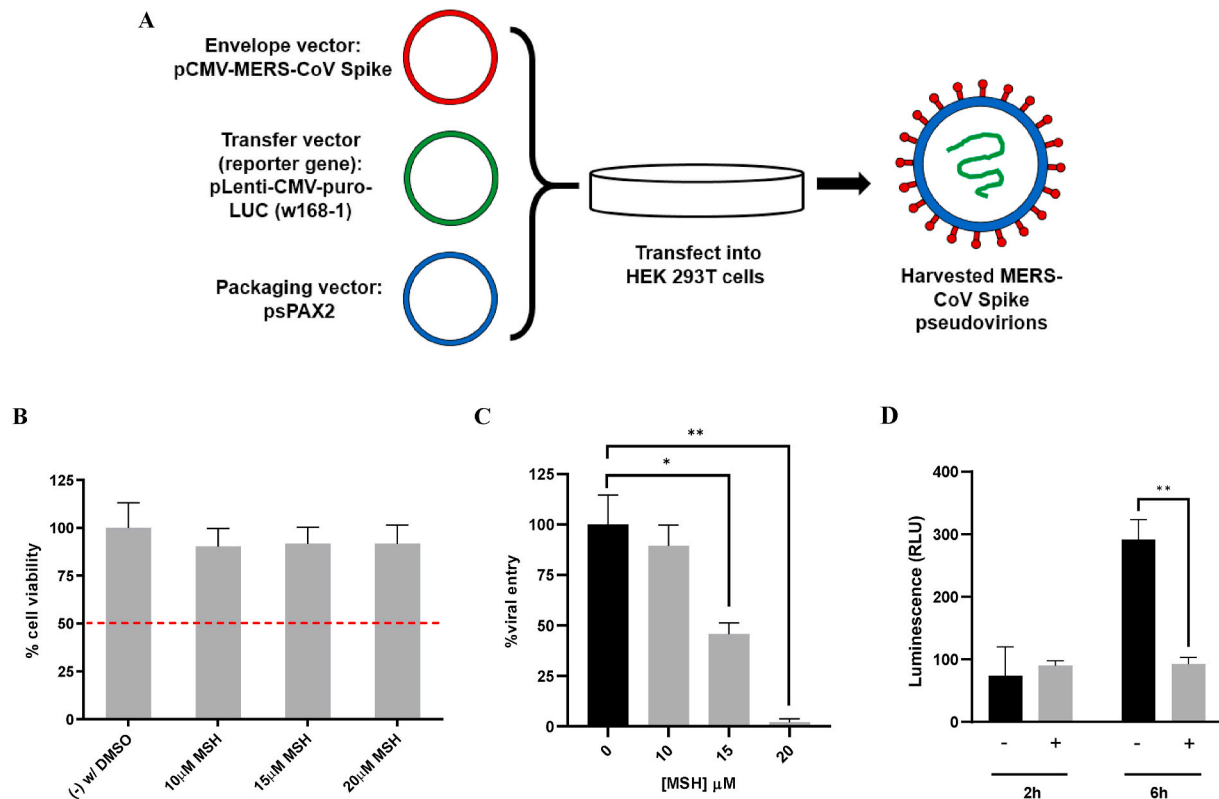
Fig. 4. Dose-dependent inhibition of MERS-Spike pseudovirion entry by MSH. (A) Schematic illustration of the lentiviral pseudotyping procedure using a 3-plasmid system – Envelope, Transfer, and Packaging vectors. (B) Cell viability assay showed that the three concentrations of MSH used for inhibition assays on *Vero E6* cells result in minimal cell death. (C) PV entry inhibition assay on *Vero E6* cells showed that 20 μM drastically inhibited viral entry compared to 10 and 15 μM. One-way ANOVA statistical analysis was performed with Dunnett's Post-hoc test to compare all columns with the control column. n = 3, *p < 0.05, **p < 0.01. (D) The time-dependent assay demonstrated specific PV entry inhibition upon 6 h treatment with 20 μM MSH and harvested 48 h post-infection (hpi). Unpaired *t*-test (one-tailed), n = 3. **p < 0.01. The error bar represents SEM.

3.2. MSH binds to MERS-CoV RBD

For binding studies, the recombinant RBD was expressed via the baculoviral expression system for the required post-translational glycosylations (Alfalah et al., 2002; Ikushima et al., 2000), followed by purification (Suppl. Figure 1, 2). Seven compounds identified from our structure-guided *in silico* screening of FDA-approved drugs were assessed for potential binding using intrinsic fluorescence quenching. Preliminary screening of these ligands was conducted at a fixed protein-ligand molar ratio of 1:5, and the appropriate negative controls were implemented (Suppl. Fig. 3A and B). Results suggested that Nalmefene (N), Cefaclor (Cef), and MSH could potentially interact with MERS-CoV RBD (Suppl. Figure 3C). Further dose-dependent titrations of these three compounds revealed prominent quenching by MSH, compared to the other two (Fig. 2, Suppl. Figure 3C). Titration data were transformed and analyzed on a binding saturation curve where the calculated K_D for MSH was 62.99 ± 7.62 μM (Fig. 2B). In an attempt to enhance protein stability and further study this interaction, Maltose-binding protein (MBP) tagged MERS-CoV RBD was prepared and used for Differential Scanning Fluorimetric (DSF) experiments with varying concentrations of MSH. Subsequent calculations reflected a K_D value of 8.41 ± 0.25 μM, which agrees with the fluorescence quenching results (Fig. 2C).

Additional mutation studies to ascertain our *in silico* modeling data was carried out. Three specific point mutations, Y540A, R542D, and V555A, were generated, followed by fluorescence quenching with MSH, and compared with the wild type construct. The study revealed that V555A exhibited a notable reduction in quenching, suggesting that the predicted hydrophobic interactions between V555A and MSH could be important for binding between MERS-CoV RBD and MSH (Fig. 2D).

Subsequent analytical gel filtration chromatography experiments on MERS-CoV RBD, DPP4, and MSH exhibited a slight but distinct and consistent peak shift in fractionation volume from the RBD-DPP4 complex peak towards the DPP4-only peak regardless of mixing order, suggesting potential inhibition and complex dissociation effects of MSH in RBD-DPP4 complex formation (Fig. 3).

3.3. MSH inhibits MERS-Spike pseudovirion (PV) entry

We then investigated the potential inhibitory effect of MSH using non-replicative pseudovirions. For the monitoring and quantitative analysis of PV entry, a luciferase reporter gene was incorporated into the PV (Fig. 4A, Suppl. Fig. 4A and B) (Grehan et al., 2015). Before the inhibition assays, the 50% cytotoxic concentration (CC_{50}) of MSH was found to be 35.1 μM (Suppl. Figure 4C). Based on this, three different MSH concentrations were systematically tested in our infection assays: 10 μM, 15 μM, and 20 μM. The toxicity screening for these selected MSH concentrations was carried out in parallel with the viral entry inhibition assay. Here, our results reflected an enhanced reduction in luciferase activity at 20 μM MSH, signifying maximum viral entry inhibition with minimal effect arising from cell death due to drug toxicity (Fig. 4B and C).

An additional time-point assay was conducted to study the time-dependent inhibitory effect of MSH. Our data reflected a significant decrease in luminescence, directly correlating to a distinct viral entry inhibition, after 6 h of treatment of 20 μM MSH (Fig. 4D). This signifies that although the PV inoculum with MSH was incubated with the cells for a short duration of 6 h before being replaced with fresh media for the subsequent 42 h before luminescence detection, it is sufficient to observe a significant decrease in PV entry. Therefore, this suggests that MSH is
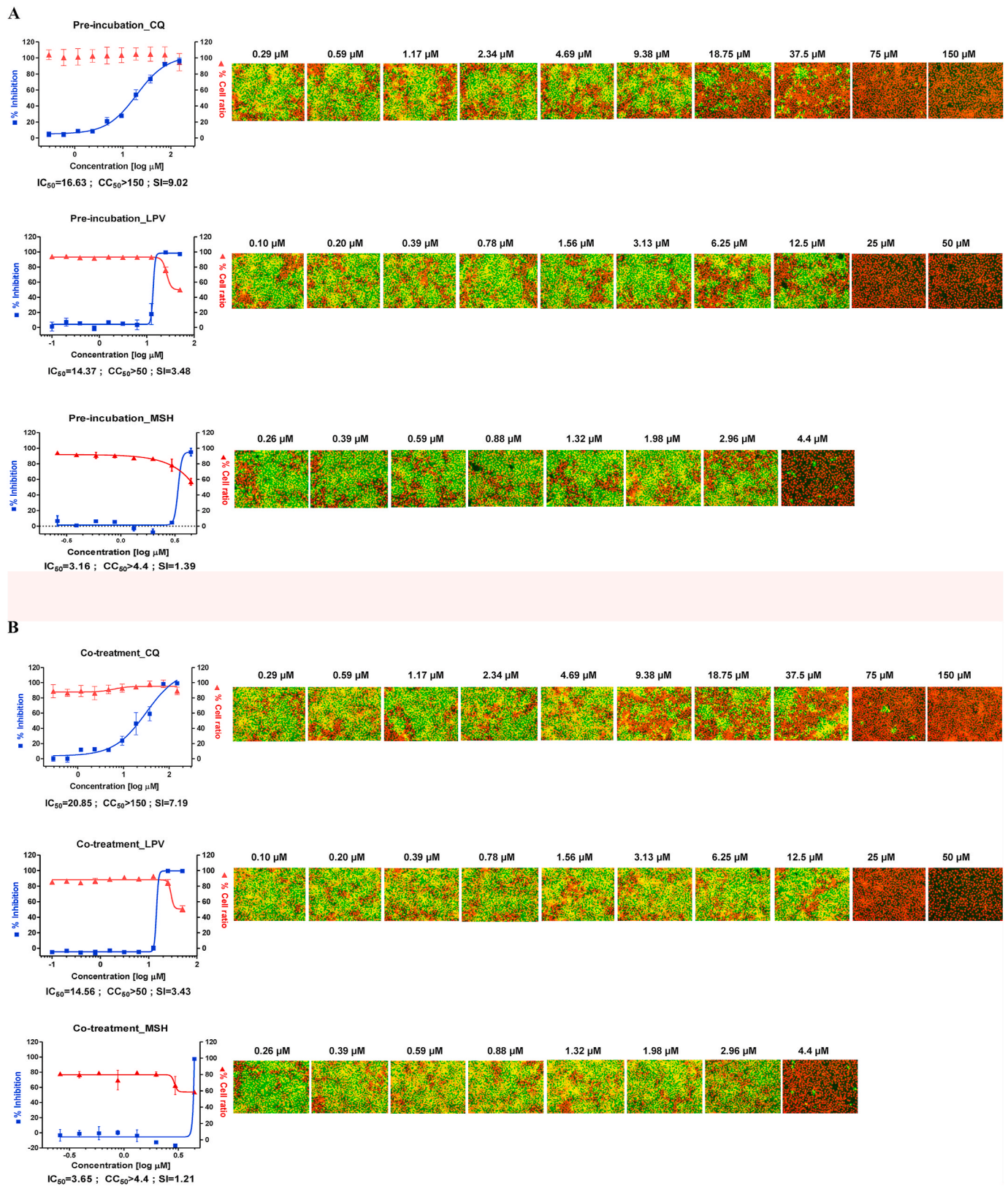
Fig. 5. Inhibitory effect of MSH on MERS-CoV infection in *Vero* cells.

Dose-response curves and immunofluorescence images of MSH addition compared to Chloroquine diphosphate (CQ) and Lopinavir (LPV) in two different conditions: (A) Pre-incubation, where MSH was mixed with MERS-CoV 1h before infection, and (B) Co-treatment, where MSH was mixed with MERS-CoV and transferred to the cells immediately. In both set-ups, viral inoculums and MSH treatment were incubated with the cells 24 h before fixation and harvesting. Points and blue lines represent the percentage of inhibition of MERS-CoV infection, and those in red refer to cell viability percentages. In the immunofluorescence images, red signals reflect viable cells, and green signals reflect viral progression.

involved in the early stages of viral infection, in line with our hypothesis that MSH targets the MERS-CoV spike glycoprotein to inhibit viral progression.

3.4. MSH attenuates MERS-CoV infection in cell culture

To validate our results from the PV assays, we performed further experiments with infectious MERS-CoV (MERS-CoV/EMC/2012) under two different conditions: Pre-incubation and Co-treatment (Fig. 5). In the pre-incubation experiment, the virus and MSH were mixed and incubated for 1 h before addition to cells. On the other hand, both virus and MSH were added to the cells simultaneously without prior incubation in the co-treatment experiment. The concentration of MSH was maintained until the infected cells were fixed for immunofluorescence imaging. As controls, chloroquine and lopinavir's antiviral efficacy were assessed in parallel (Chan et al., 2015). The IC_{50} of MSH with the infectious MERS-CoV was determined by the dose-response curve (DRC) analysis. It was approximately 3 μM in both pre-incubation and co-treatment experiments (Fig. 5). This IC_{50} value was substantially lower than those with chloroquine and lopinavir, suggesting a more potent antiviral efficacy of MSH against infectious MERS-CoV.

4. Discussion

Due to the lack of vaccines and drugs against MERS, there is a critical need for research and therapeutic discovery and development. Such studies are vital, as we cannot ignore the possibility of a mutant form of MERS emerging in the future, such as SARS-CoV2 from SARS-CoV. In this direction, structure-guided *in silico* screening of FDA-approved drug libraries was conducted, revealing seven potential hits. Intrinsic fluorescence quenching titrations performed using recombinant MERS-CoV RBD samples showed a significant dose-dependent quenching effect upon MSH addition. In addition to the substantial quenching of fluorescence signals, a red-shift in the emission maxima was observed upon increasing MSH concentration. This red-shift correlates to a conformational change to an increasingly polar microenvironment (Akbar et al., 2016; Di Bartolo, 2013; Möller and Denicola, 2002). Further studies conducted with DSF agreed with our previous quenching analyses, which revealed that MSH is a potential U-binder, resulting in destabilizing interactions with MERS-CoV RBD (Cimmperman et al., 2008). Structure elucidation attempts were performed using co-crystallization and soaking methods, but diffraction data and analysis revealed the absence of the inhibitor electron density, indicating the requirement for further optimization.

Cell-based PV infection assays demonstrated a significant inhibitory effect exerted on PV entry. The current hypothesis is that MSH interacted with the RBD on the MERS-CoV Spike glycoproteins, which then inhibited RBD/DPP4 complex formation and, consequentially, viral entry inhibition. A limitation of PV studies is the absence of co-factors and proteins on the virion surface, which might help compensate or strengthen viral attachment (Jolly and Sattentau, 2013). As such, the infectious virus isolated from MERS-infected patients were used in subsequent inhibition assays on *Vero* cells.

MSH cytotoxicity screens were conducted before cell-based assays with infectious MERS-CoV to ascertain any reduction in the viral progression due to MSH's inhibitory effect. Moreover, MSH was identified as a potent inhibitor of viral entry as it exhibited a more robust response observed with the pseudovirion experiments. Calculations from our infectious MERS-CoV assays revealed an IC_{50} of ~3 μM, comparatively more potent to LPV, which is currently used in clinical trials as part of the MIRACLE trial for MERS-CoV (Chan et al., 2015). Although the calculated IC_{50} falls in the μM range compared to other therapeutic compounds (nM to pM ranges), MSH still exhibited potent viral entry inhibition (Makau et al., 2017).

A future study to examine the effect of MSH on MERS-CoV infection in DPP4 transgenic mice models would be an ideal way forward

(Coleman et al., 2014; Li et al., 2017). Besides, a structure-based drug design approach could be adopted, wherein the structure elucidation of MSH with RBD followed by the design of MSH analogs and characterization will enable us to improve MSH potency.

In summary, in this study, we showed that the anti-asthma drug – MSH, a leukotriene D4 receptor antagonist, could bind to MERS-CoV RBD and inhibit viral progression, suggesting that MSH could be considered as a potential therapeutic lead for MERS-CoV infections.

References

Akbar, S.M., Sreeramulu, K., Sharma, H.C., 2016. Tryptophan fluorescence quenching as a binding assay to monitor protein conformation changes in the membrane of intact mitochondria. J. Bioenerg. Biomembr. 48, 241–247. https://doi.org/10.1007/s10863-016-9653-0.

Alfalah, M., Jacob, R., Naim, H.Y., 2002. Intestinal Dipeptidyl peptidase IV is efficiently sorted to the apical membrane through the concerted action of N-andO-Glycans as well as association with lipid microdomains. J. Biol. Chem. 277, 10683–10690. https://doi.org/10.1074/jbc.M109357200.

CDC, 2015. Middle East respiratory syndrome coronavirus outbreak in the Republic of Korea, 2015. Osong Public Health Res Perspect 6, 269–278. https://doi.org/10.1016/j.phrp.2015.08.006.

Chan, J.F.-W., Yao, Y., Yeung, M.-L., Deng, W., Bao, L., Jia, L., Li, F., Xiao, C., Gao, H., Yu, P., 2015. Treatment with lopinavir/ritonavir or interferon-β1b improves outcome of MERS-CoV infection in a nonhuman primate model of common marmoset. The Journal of infectious diseases 212, 1904–1913. https://doi.org/10.1093/infdis/jiv392.

Cho, H., Excler, J.-L., Kim, J.H., Yoon, I.-K., 2018. Development of Middle East respiratory syndrome coronavirus vaccines–advances and challenges. Hum. Vaccines Immunother. 14, 304–313. https://doi.org/10.1080/21645515.2017.1389362.

Cimmperman, P., Baranauskiene, L., Jachimoviciūte, S., Jachno, J., Torresan, J., Michailoviene, V., Matuliene, J., Sereikaite, J., Bumelis, V., Matulis, D., 2008. A quantitative model of thermal stabilization and destabilization of proteins by ligands. Biophys. J. 95, 3222–3231. https://doi.org/10.1529/biophysj.108.134973.

Coleman, C.M., Matthews, K.L., Goicochea, L., Frieman, M.B., 2014. Wild-type and innate immune-deficient mice are not susceptible to the Middle East respiratory syndrome coronavirus. The Journal of general virology 95, 408. https://doi.org/10.1099/vir.0.060640-0.

Di Bartolo, B., 2013. Introduction to Fluorescence Spectroscopy with Applications to Biological Systems. Springer Netherlands, Dordrecht, pp. 91–117. https://doi.org/10.1007/978-94-007-5313-6_6.

Du, L., Zhao, G., Kou, Z., Ma, C., Sun, S., Poon, V.K., Lu, L., Wang, L., Debnath, A.K., Zheng, B.-J., 2013. Identification of a receptor-binding domain in the S protein of the novel human coronavirus Middle East respiratory syndrome coronavirus as an essential target for vaccine development. J. Virol. 87, 9939–9942. https://doi.org/10.1128/JVI.01048-13.

Dyall, J., Coleman, C.M., Hart, B.J., Venkataraman, T., Holbrook, M.R., Kindrachuk, J., Johnson, R.F., Olinger, G.G., Jahrling, P.B., Laidlaw, M., 2014. Repurposing of clinically developed drugs for treatment of Middle East respiratory syndrome coronavirus infection. Antimicrob. Agents Chemother. 58, 4885–4893. https://doi.org/10.1128/AAC.03036-14.

Grehan, K., Ferrara, F., Temperton, N., 2015. An optimised method for the production of MERS-CoV spike expressing viral pseudotypes. Methods (Orlando) 2, 379–384. https://doi.org/10.1016/j.mex.2015.09.003.

Ikushima, H., Munakata, Y., Ishii, T., Iwata, S., Terashima, M., Tanaka, H., Schlossman, S.F., Morimoto, C., 2000. Internalization of CD26 by mannose 6-phosphate/insulin-like growth factor II receptor contributes to T cell activation. Proc. Natl. Acad. Sci. Unit. States Am. 97, 8439–8444. https://doi.org/10.1073/pnas.97.15.8439.

Jolly, C.L., Sattentau, Q.J., 2013. Attachment factors. Adv. Exp. Med. Biol. 790, 1–23. https://doi.org/10.1007/978-1-4614-7651-1_1.

Jones, G., Willett, P., Glen, R.C., Leach, A.R., Taylor, R., 1997. Development and validation of a genetic algorithm for flexible docking. J. Mol. Biol. 267, 727–748. https://doi.org/10.1006/jmbi.1996.0897.

Li, K., Wohlford-Lenane, C.L., Channappanavar, R., Park, J.-E., Earnest, J.T., Bair, T.B., Bates, A.M., Brogden, K.A., Flaherty, H.A., Gallagher, T., 2017. Mouse-adapted MERS coronavirus causes lethal lung disease in human DPP4 knockin mice. Proc. Natl. Acad. Sci. Unit. States Am. 114, E3119–E3128. https://doi.org/10.1073/pnas.1619109114.

Majumder, M.S., Brownstein, J.S., Finkelstein, S.N., Larson, R.C., Bourouiba, L., 2017. Nosocomial amplification of MERS-coronavirus in South Korea, 2015. Trans. R. Soc. Trop. Med. Hyg. 111, 261–269. https://doi.org/10.1093/trstmh/trx046.

Makau, J.N., Watanabe, K., Ishikawa, T., Mizuta, S., Hamada, T., Kobayashi, N., Nishida, N., 2017. Identification of small molecule inhibitors for influenza a virus using in silico and in vitro approaches. PloS One 12. https://doi.org/10.1371/journal.pone.0173582.

Möller, M., Denicola, A., 2002. Protein tryptophan accessibility studied by fluorescence quenching. Biochem. Mol. Biol. Educ. 30, 175–178. https://doi.org/10.1002/bmb.2002.494030030035.

NCBI, 2020. PubChem Compound Database. CID=71311637.

Park, J.W., Lee, K.J., Lee, K.H., Lee, S.H., Cho, J.R., Mo, J.W., Choi, S.Y., Kwon, G.Y., Shin, J.-Y., Hong, J.Y., 2017. Hospital outbreaks of middle east respiratory syndrome, Daejeon, South Korea. Emerg. Infect. Dis. 23, 898. https://doi.org/10.3201/eid2306.160120, 2015.

Perlman, S., Vijay, R., 2016. Middle East respiratory syndrome vaccines. Int. J. Infect. Dis. 47, 23–28. https://doi.org/10.1016/j.ijid.2016.04.008.

Raj, V.S., Mou, H., Smits, S.L., Dekkers, D.H., Müller, M.A., Dijkman, R., Muth, D., Demmers, J.A., Zaki, A., Fouchier, R.A., 2013. Dipeptidyl peptidase 4 is a functional receptor for the emerging human coronavirus-EMC. Nature 495, 251–254. https://doi.org/10.1038/nature12005.

Sharif-Yakan, A., Kanj, S.S., 2014. Emergence of MERS-CoV in the Middle East: origins, transmission, treatment, and perspectives. PLoS Pathog. 10 https://doi.org/10.1371/journal.ppat.1004457 e1004457-e1004457.

Song, Y.-J., Yang, J.-S., Yoon, H.J., Nam, H.-S., Lee, S.Y., Cheong, H.-K., Park, W.-J., Park, S.H., Choi, B.Y., Kim, S.S., 2018. Asymptomatic Middle East Respiratory Syndrome coronavirus infection using a serologic survey in Korea. Epidemiology and health 40. https://doi.org/10.4178/epih.e2018014.

Sterling, T., Irwin, J.J., 2015. ZINC 15–ligand discovery for everyone. J. Chem. Inf. Model. 55, 2324–2337. https://doi.org/10.1021/acs.jcim.5b00559.

Systèmes, D., 2016. BIOVIA, BIOVIA Discovery Studio, 4.0. Dassault Systèmes, San Diego.

Wang, N., Shi, X., Jiang, L., Zhang, S., Wang, D., Tong, P., Guo, D., Fu, L., Cui, Y., Liu, X., 2013. Structure of MERS-CoV spike receptor-binding domain complexed with human receptor DPP4. Cell Res. 23, 986. https://doi.org/10.1038/cr.2013.92.

WHO, 2018. 2018 Annual Review of Diseases Prioritized under the Research and Development Blueprint. Geneva, Switzerland.

WHO, 2020. MERS Situation Update. January 2020.

Zaki, A.M., Van Boheemen, S., Bestebroer, T.M., Osterhaus, A.D., Fouchier, R.A., 2012. Isolation of a novel coronavirus from a man with pneumonia in Saudi Arabia. N. Engl. J. Med. 367, 1814–1820. https://doi.org/10.1056/NEJMoa1211721.

Zhang, N., Jiang, S., Du, L., 2014. Current advancements and potential strategies in the development of MERS-CoV vaccines. Expet Rev. Vaccine 13, 761–774. https://doi.org/10.1586/14760584.2014.912134.

Zhou, Y., Yang, Y., Huang, J., Jiang, S., Du, L., 2019. Advances in MERS-CoV vaccines and therapeutics based on the receptor-binding domain. Viruses 11, 60. https://doi.org/10.3390/v11010060.